**ChemElectroChem**

Research Article
doi.org/10.1002/celc.202200891

**Chemistry Europe**
European Chemical
Societies Publishing

www.chemelectrochem.org
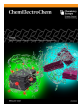
# Critical Analysis of MXene Production with In-Situ HF Forming Agents for Sustainable Manufacturing

Antonio Gentile,[a, b] Stefano Marchionna,[b] Marcella Balordi,[b] Gioele Pagot,[c, d] Chiara Ferrara,*[a, d] Vito Di Noto,[c, d] and Riccardo Ruffo[a, d]

MXenes are an emerging class of materials considered for many applications, such as sensors, catalysis, energy storage devices. The main obstacle towards their massive implementation is the synthesis requiring the direct use of HF as etching agent. The development of alternative synthetic routes exploiting in-situ forming HF agents is the main strategies to overcome this limitation. In this study four different etching methods based on the use of $NH_4HF_2$, NaF—HCl, $HBF_4$, and $NaBF_4$—HCl are compared to produce $Ti_3C_2T_x$ from $Ti_3AlC_2$ towards the application of MXenes in sodium ion batteries. Three of such etching methods have already been reported while one is here presented for the first time. The structural analysis of the obtained products is based on X-ray diffraction (XRD), scanning electron microscopy-energy dispersive X-ray spectroscopy (SEM-EDX), and X-ray photoelectron spectroscopy (XPS) analysis. All the materials have been tested in half-cell configuration vs. Na; the charge/discharge profiles and the C-rate tests are discussed and related to specific structural features. Overall, the results reveal that the MXene obtained using the $HBF_4$ etching agent under mild conditions is comparable both in structure and functional properties to the benchmark material, i.e., the MXene produced using HF at 5% concentration. Indeed, the MXene synthetized with the $HBF_4$ presents the lowest mean voltage and potential hysteresis and shows the highest first cycle efficiency (69.7%), overcoming the performance of the MXene produced with 5% HF (67%). This study proves the possibility to produce MXene with a more sustainable route.

## Introduction

The development of two-dimensional (2D) materials is a field in continuous expansion finding more and more applicative sectors thanks to the peculiar optical, electronic, thermal, and mechanical properties of such materials.[1–3] Although 2D materials should be single layer by rigorous definition, in many case the presence of free hanging bonds/high energy sites on the surface of the layers can lead to the aggregations of dozens of layers with the formation of pseudo-bulk structures that resemble three-dimensional (3D) layered materials. However, the properties of these two families of materials are very different, because in the 2D pseudo-bulk materials the functional properties are determined by the internal surfaces between the lamellae, which have chemical-physical characteristics more similar to those of chemically functionalized surfaces than of ordered atomic structures (3D layered materials). A noteworthy and emerging example of these materials are the MXenes, a class of 2D materials with $M_{n+1}X_nT_x$ formula based on $M_{n+1}X_n$ lamellae (n ranging from 1 to 2) with T terminal groups attached on the surface, as seen in Figure 1 with M=Ti, X=C, n= 2. The nature of the $M_{n+1}X_n$ lamellae depends on the precursor used for the synthesis while the T terminations depend on the synthesis conditions. Indeed, the MXene are synthesized by the MAX phase precursor $M_{n+1}AX_n$ in which M is a transition metal (e.g., Ti, Cr, V, Mo, Nb), A can be an element from group 13 or 14 (mainly Al or Si), X can be carbon (C), or nitrogen (N) or a mixture of the two.[4,5] The MAX phase can be described as 3D layered structures (space group $P6_3/mmc$) in which the atoms arrange along the c axis with a repetition of $M_{n+1}X_n$ layers spaced by A planes (Figure 1a).[6–8] The MXenes can be obtained from the MAX phases through the selective removal of the A element, generally obtained via etching. This procedure involves the substitution of the A element with terminal groups T. The chemical nature and relative percentage of different species of the terminations can be partially controlled through the selection of the etching agent (HF, HF generating agents, molten salts)[9–12] and with subsequent chemical modifications[13] resulting in —O, —OH, —F, —Cl, —Br, —I, —S, —NH groups. Due to the peculiar synthesis, the MXene maintains the same MAX phase lamellar nature, with each lamella made by a

[a]  Dr. A. Gentile, Dr. C. Ferrara, Prof. R. Ruffo
Department of Materials Science
University Milano Bicocca
via Cozzi 55, 20125 Milano, Italy
E-mail: chiara.ferrara@unimib.it

[b]  Dr. A. Gentile, Dr. S. Marchionna, Dr. M. Balordi
Ricerca sul Sistema Energetico, RSE S.p.A.
Via R. Rubattino 54, 20134 Milano, Italy

[c]  Dr. G. Pagot, Prof. V. Di Noto
Section of Chemistry for the Technology (ChemTech), Department of Industrial Engineering
University of Padova
Via Marzolo 9, PD, I-35131 Padova, Italy

[d]  Dr. G. Pagot, Dr. C. Ferrara, Prof. V. Di Noto, Prof. R. Ruffo
National Reference Center for Electrochemical Energy Storage (GISEL)
Consorzio Interuniversitario Nazionale per la Scienza e Tecnologia Dei Materiali (INSTM)
via Giusti 9, 50121 Firenze, Italy

**ChemElectroChem**

Research Article
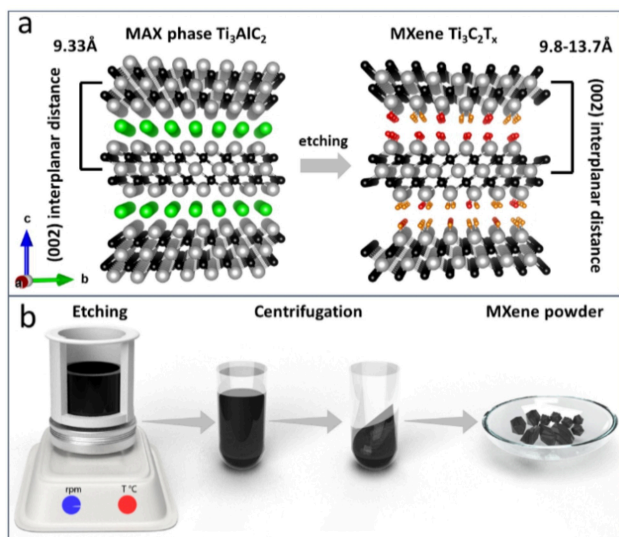doi.org/10.1002/celc.202200891

Chemistry
Europe
European Chemical
Societies Publishing

**Figure 1.** (a) Crystalline structure of the MAX phase ($Ti_3AlC_2$) and MXene ($Ti_3C_2F_x$) functionalized after etching (Ti grey, C black, Al green, F orange, O red). The treatment produced an increase of the interlayer distance along the c parameter due to new functionalization instead of aluminum. (b) Schematic process of etching for the production of MXene phase.

repetition of $[T_x(M_{n+1}X_n)T_x]_k$ stacks.[14] As described above, the interlayers' interactions (dipolar and Van der Waals) related to the presence of terminal groups lead to formation of aggregated 2D bulk particles.[8] However, depending on the nature and stoichiometry of the T groups, this situation can be modulated and the weakness of the T···T interlayers' interactions leads to the formation of larger and accessible interlayer spaces. Moreover, thanks to the terminations, MXenes are extremely polar and can be easily delaminated and dispersed in both aqueous and organic polar solvents.[15,16]

The high-surface delaminated MXene sheets have be used in gas storage,[17] as photo-[18] or electro-catalyst,[19,20] in water desalination,[21,22] and in electrochemical capacitors and re-chargeable batteries.[5,23,24] Specifically, the optimal interlayer distance and other beneficial properties of the MXene such as high electrical conductivity, good mechanical properties, and flexibility, make this class of compounds extremely suitable for this latter application. Furthermore, the dipolar interactions between these $T_x$ groups do not allow the flaking or pulverization of the particles during the intercalation and deintercalation processes of the ions. The system, in fact, reacts to the movement of ions by reversibly adapting the interplanar distance.[23,25] Despite the multiple options regarding the substitution of elements M, A, and X, the most studied and used MXene is the $Ti_3C_2T_x$ phase, given the relative ease of etching of the corresponding precursor $Ti_3AlC_2$. The most common and exploited way to produce $Ti_3C_2T_x$ from $Ti_3AlC_2$ is the etching in hydrofluoric acid or in acid solutions containing fluoride ions.[5,9,11] For these specific reactions, the T groups introduced on the MXene layers can be −O, −OH, −F, i.e., all the anions present in the etching bath. $Ti_3C_2T_x$ was proposed as anode for sodium ion batteries due to the scarcity of materials able to reversible intercalate sodium ions at low potential vs.

the $Na^+$/Na couple. Despite the modest specific capacity, ranging from 110 to 150 $mAhg^{-1}$ in massive electrodes, the $Ti_3C_2T_x$ phase can be used for hundreds of cycles with very high Coulomb efficiency ($>99.5\%$ at low current) and 100% capacity retention.[14] Given these interesting results as well as the great variety of applications of the $Ti_3C_2T_x$ phase, it is therefore important to make the production process simple, scalable, and globally more sustainable. The synthesis of these 2D materials, indeed, remains the bottleneck for the large production and application of the MXenes in different fields, due to the use of hydrofluoric acid, which is toxic, difficult to handle, and requires dedicated apparatus and facilities. Although examples of mini-plants that can produce the $Ti_3C_2T_x$ phase in amount of industrial interest are already present,[26] the process simplifica-tion is mandatory and the use of HF low concentrated solutions or of reagent mixtures able to form HF in situ is desirable. There are, indeed, only a few examples of MXene production through HF free processes and such as hydrothermal reactions in NaOH 27 M (Bayer method),[27] the use of molten salts at high temperatures,[28,29] the use of ionic liquid[30] or use of precursors forming HF in situ.[5] While the hydrothermal method and use of molten salts involve the use of harsh conditions, the in-situ generation of HF can be considered as a profitable way to dump the overall hazard of the synthesis. As already discussed, the etching agent and the synthesis conditions strongly influence the nature of the T terminations, the amount of impurities, and the presence of intercalated species. Moreover, the microstructural and morphological characteristics of the final product are also dependent on the same parameters. All these aspects, in tuns, have strong impact on the electro-chemical properties of the materials and must be thus controlled.[31]

In this work we compare four different etching routes to obtain $Ti_3C_2T_x$ starting from the MAX phase precursor. The four etching solutions are based on: i) $NH_4HF_2$, ii) NaF in HCl, iii) $HBF_4$, and iv) $NaBF_4$ in HCl. The reactions occurred for the in-situ formation of HF in these four etching solutions are described as Equations 4–14. While the $NH_4HF_2$, NaF in HCl, and $NaBF_4$ in HCl have already been reported, here we propose for the first time the use of the $HBF_4$ as etching agent; moreover, we optimized the procedure for the other three methods. In the literature some examples of MAX phase etching in NaF in HCl[31] and $NH_4HF_2$[32] have been reported and there is only one example of the MXene production in a $NaBF_4$ and HCl[33] solution through a hydrothermal synthesis at 180°C, but this experimental setting involves the complete dissolution of the salt and the formation of HF in solution. To make less corrosive and safer the reaction environment, in this work we operated at low temperature in order to exploit directly $HBF_4$ as an etching species and not relying only on the HF produced by its decomposition. There are studies showing that $HBF_4$ is an acid that can be used as a substitute for HF in many synthetic processes, such as acid digestions or silica etching on silicon wafers or piezoelectric materials.[34] Under these conditions, the kinetics of degradation and formation of HF, however, is slower than the hydrothermal reaction,[35] so in this work it was assessed if $HBF_4$ species can

**ChemElectroChem**

Research Article
doi.org/10.1002/celc.202200891

**Chemistry
Europe**

European Chemical
Societies Publishing

be considered, like the previous ones, an etching agent for $Ti_3AlC_2$.

This study is aimed to compare the structural, morphological, and electrochemical properties of the obtained MXenes and to rationalize the effect of the etching agent on their properties. The electrochemical performances are referenced to those of the $Ti_3C_2T_x$ obtained by our group with direct use of HF 5 wt% with optimized etching procedure[14,36] considered here as the benchmark. With the present work we demonstrate that the MXene obtained exploiting the $HBF_4$ as etching agent shows electrochemical properties similar to those of our standard. The more sustainable route for the MXene production can be considered as a valid alternative to the direct HF etching, opening the way for the massive production of such material. All the materials have been analyzed and characterized by X-ray diffractometry, the morphology by scanning electron microscopy, the composition by elemental analysis (CHNS) and X-ray photoelectron spectroscopy (XPS) analysis and the performance in sodium ion cells by galvanostatic cycling with potential limitation.

## Results and Discussion

The X-ray diffraction (XRD) profiles of MX_NaF_HCl, MX_NH$_4$HF$_2$, MX_HBF$_4$ and MX_NaBF$_4$_HCl are presented and compared in Figure 2 and in Table 1 together with the details of the preparation; the experimental patterns are compared with an MXene produced in HF 5% wt HF (MX_HF$_{5\%}$) and the precursor MAX phase for which a detailed analysis has performed by our group and results have been reported in previous works.[14,36] The obtained patterns demonstrate that all the considered etching solutions can be exploited to successfully obtain the complete conversion of the MAX phase into the MXene under the considered and optimized experimental conditions. This can be inferred from the downshift of the 002 peak (9.5° for the MAX phase) to lower angles (7°–9° depending on the samples) which can be associated with the increase in interplanar distance due to the replacement of Al layers in the MAX phase with 2 layers of $T_x$ terminations (Figure 1a). The (10 $l$) reflections, well resolved and sharp for the MAX phase, are blurred and differently broadened for the four MXenes; this peculiar effect is associated with the loss of diffracting coherence among the layers and is considered as identifier of successful etching of the MAX phase.[37,38] All the etching solutions can be thus
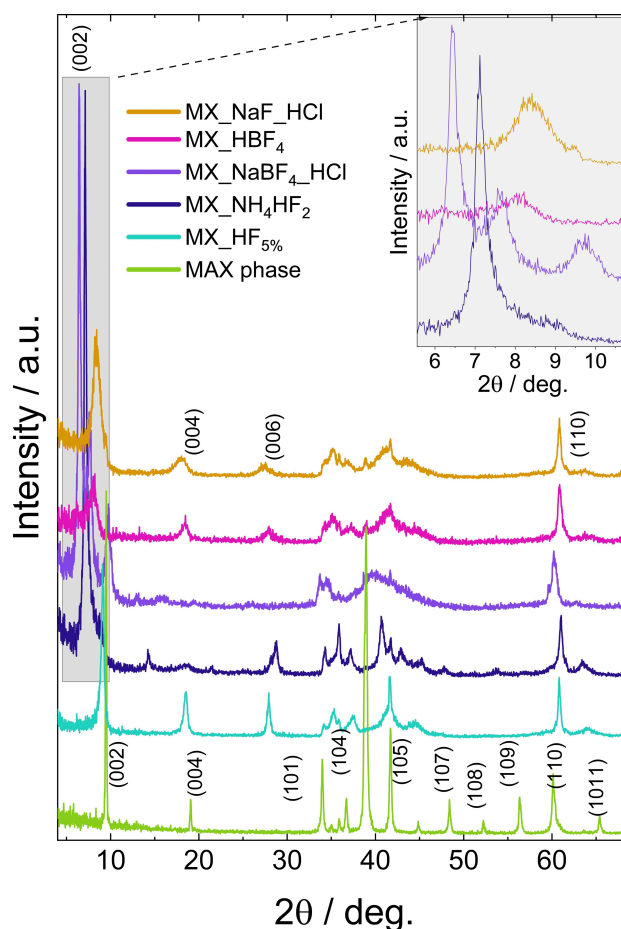


**Figure 2.** XRD patterns of all the MXenes produced in the work compared to Max phase precursor and MXene produced with traditional HF-etching and zoom in the 5-11 deg. in the insert.

exploited for the preparation of the MXene from the MAX phase. At the same time a closer inspection of the patterns reveals that the obtained products are different, and the characteristic features depend on the etching method explored. Indeed, the basal interplanar distance calculated from the angular position of the (002) peak is strongly influenced by the type of etching solution; the values of the interplanar distance calculated by means of the Bragg law are reported in Table 2.

Generally, for all the explored etching solution, the obtained MXenes have larger interlayer distance with the respect to the reference MX-HF$_{5\%}$. The observed trend is in good agreement

**Table 1.** List of samples and experimental parameters considered for the etching procedure.

| Sample | Etching agent | Nominal max HF concentration [%w]* | Time and temperature [h/°C] | Synthesis yield [%]** |
|---|---|---|---|---|
| MX_HF$_{5\%}$ | HF | 5.0 | 24/25 | 95 |
| MX_NH$_4$HF$_2$ | NH$_4$HF$_2$ | 3.5 | 24/40 | 90 |
| MX_NaF_HCl | NaF in/HCl | 4.0 | 24/40 | 94 |
| MX_HBF$_4$ | HBF$_4$ | 18.3 | 24/60 | 71 |
| MX_NaBF$_4$_HCl | NaBF$_4$ in HCl | 7.3 | 24/60 | 65 |

[*] The calculated HF concentration is the maximum value obtainable considering the Reactions 4–14 presented in the Experimental Section completed. Actually, this cannot be obtained under the experimental conditions considered, especially for the HBF$_4$ and NaBF$_4$ systems. The values have been calculated to allow a direct and easy comparison among the etching solutions. [**] The yields are referred to the synthesis process and not to the conversion process and have been calculated on the base of the weight of the powders as described in Equation 15.

**ChemElectroChem**

Research Article
doi.org/10.1002/celc.202200891

**Chemistry Europe**
European Chemical
Societies Publishing

**Table 2.** Cell parameters in relation to 002 peaks position and reference values where available for the 2θ peak positions. The size of the diffracting domains has been estimated from the broadening of the 002 peak using the Sherrer equation.

| Sample | 2θ [deg.] | d(002) [nm] | Unit cell c [nm] | 2θ ref. [deg.] | Crystallite size [nm] |
|---|---|---|---|---|---|
| MAX phase[34,35] | 9.55 | 0.93 | 1.85 | | 58 |
| MX_HF$_{5\%}$[34,35] | 9.10 | 0.97 | 1.94 | | 21 |
| MX_NH$_4$HF$_2$ | 7.16 | 1.23 | 2.47 | 7.15[31] | 28 |
| MX_NaF_HCl | 8.40 | 1.05 | 2.10 | 7.48[39] | 6.4 |
| MX_HBF$_4$ | 8.06 | 1.10 | 2.19 | | 7.2 |
| MX_NaBF$_4$_HCl | 6.43 | 1.37 | 2.75 | 7.1[33] | 29 |

with the trend obtained from literature value.[31,33,39] The variability among the samples is rationalized considering that the interlayer spacing is determined by the nature of T terminations and also by the interlayer species that can be trapped/stored during the etching reactions, as already described.[14,36] The use of in-situ HF forming agents involved the presence of cations and anions and molecules in the etching medium such as $Cl^-$, $Na^+$, $NH_4^+$, $H_3BO_3$ that have already been observed to be trapped within the layers, resulting in expanded spacing. The presence of intercalated species can affect the kinetic of the etching reaction and also the electrochemical properties, altering the Na intercalation/deintercalation mechanism.

The etching procedure also affects the degree of disorder of the layered materials; this can be inferred from the blurring of several reflections of the (10 *l*) class in the 30°–50° angular range, as widely discussed previously by our group.[36] Considering the 002 reflection, the broadening is also associated to the thicknesses of the coherent crystalline domains inside the lamellae along the c axis. The simple application of the Scherrer formula leads to thicknesses and estimation of particles size that are reported in Table 2. For the MX_NaBF$_4$_HCl, a peculiar situation is detected as three different peaks are observed. This can be associated to a multimodal distribution of interlayer distances and thus to different populations of particles and/or layers with different interlayer content.[40] This sample is also characterized by the merging of the (10 *l*) reflection; thus, it can be concluded that the etching reaction is complete, but a mixture of different products is obtained. This hypothesis is supported by the XPS data showing that no Al is detected for the present sample, confirming that the MAX conversion into the MXene has been completed. XPS analysis also reveals the presence of chlorine; the introduction of −Cl as possible termination can be correlated with the presence of a multimodal distribution of interlayer distances.

The differences revealed at structural level are detected also at higher scale in the morphology of the products, as evident from the scanning electron microscopy (SEM) images reported in Figure 3 for the different MXenes and the starting MAX phase. The compact lamellar morphology of the MAX phase is preserved only for the MX_NaF_HCl product, that is the sample showing the lower interplanar distance. In the other cases the morphology becomes accordion-like, with open 2D structure in
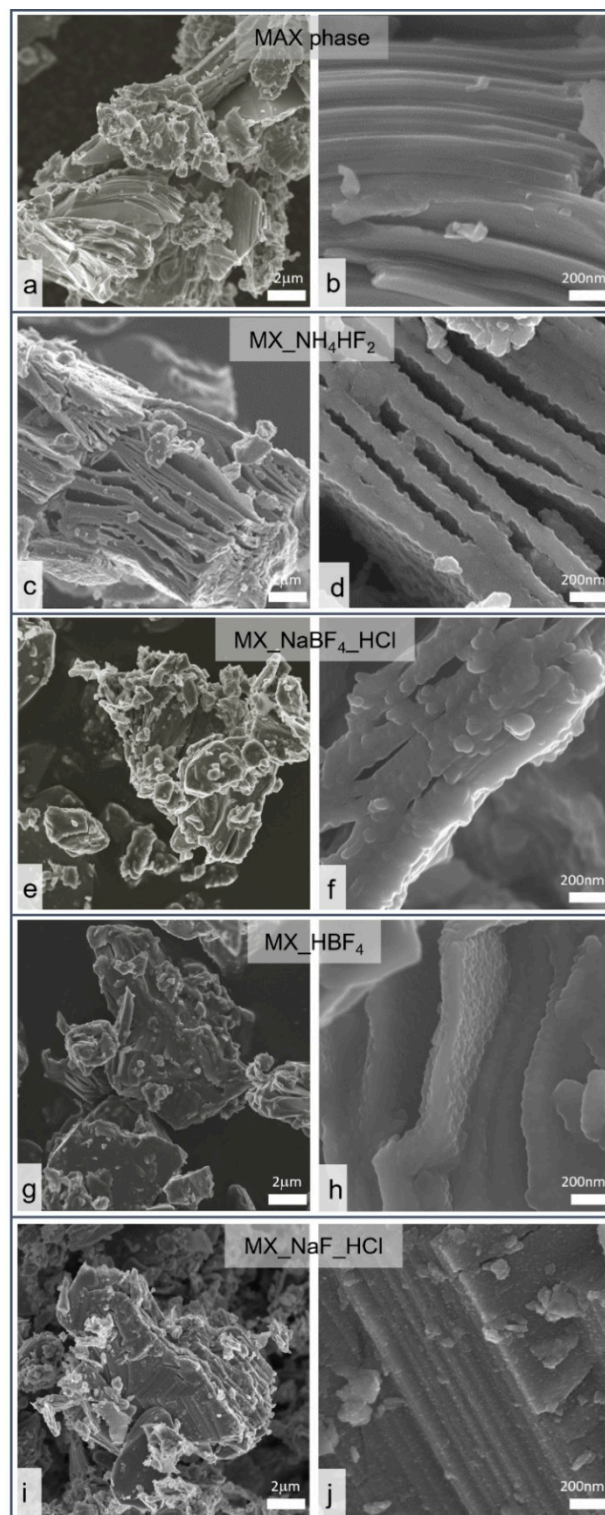


**Figure 3.** SEM images of: (a, b) MAX phase; (c, d) MX_NH$_4$HF$_2$; (e, f) MX_NaBF$_4$_HCl; (g, h) MX_HBF$_4$; (i, j) MX_NaF_HCl at different magnifications.

particular for the MX_NH$_4$HF$_2$ composition. The lamellae have an average thickness of 150–200 nm for all the samples and different degree of surface roughness. This final aspect could be associated with the presence of impurities or with partial molten materials, in particular amorphous and nanometric TiO$_2$-

**ChemElectroChem**

Research Article
doi.org/10.1002/celc.202200891

**Chemistry
Europe**
European Chemical
Societies Publishing

$_x F_{2x}$ particles formed following the exothermic reaction between hydrofluoric acid and aluminum and already observed for similar compositions.[14,36,41] The considered etching methods thus allow to obtain different morphology as the NaF/HCl solution leads to the formation of a compact MXene structure while the use of $NH_4HF_2$ solution allows for the formation of open 2D system.

The obtained MXenes have been characterized also in terms of chemical composition; the elemental composition from CHNS analysis is reported in Table 3. All the materials do not show significant carbon losses compared to the MXene theoretical composition. The exact stoichiometry of MXene cannot be defined because its general formula is $Ti_3C_2F_xO_y(OH)_z$ with undefined stoichiometry with respect to the terminations. It has been shown that the −OH functionalizations are generally lost in favor of −O functionalizations[38] and that a full coverage of the termination T sites is expected based on thermodynamic stability evaluation.[42–44] On these bases, a $Ti_3C_2FO$ stoichiometry can be considered as the average reference composition and thus the percentages of titanium, carbon, fluorine, and oxygen should be respectively 70.88 wt%, 11.85 wt%, 9.35 wt%, and 7.89 wt%. Considering the data in Table 3, the amount of carbon for all the samples is comparable to the theoretical quantity expected for the material, thus confirming the successful synthesis. All the MXenes have a modest amount of hydrogen, produced by Reactions 1–3; evidence of the trapping of $H_2$ within the lamellae have already been reported by our group.[14] For the MX_$NH_4HF_2$ sample 0.61 w% of nitrogen is detected; this is further evidence of the presence of ammonium ions that intercalates in the structure during the etching, as already reported for similar system.[31]

To further explore the composition of the MXenes and highlight the effects of the different etching agents, XPS analysis have been performed on all the samples, the main results are reported in Figure 4. The complete removal of Al from the MAX phase has been verified as in our previous work by the absence of the characteristic Al signal at 74 eV in the XPS portion (data not shown), in agreement with previous studies,[14,45] confirming once again the effectiveness of the etching methods. Considering the MXene building blocks, the Ti−C layers, the Ti and C spectra are reported in Figure 4.

All the Ti 2p spectra can be fitted with four couples of peaks (due to the spin-orbit splitting), each one attributed to titanium species with an increasing oxidation state. In particular, for the Ti $2p_{3/2}$ peaks: (i) at *ca.* 454.8 eV the $Ti^{1+}$ signal is observed; (ii) the peak centered at *ca.* 455.6 eV is attributed to $Ti^{2+}$ species; (iii) the $Ti^{3+}$ contribution appears at *ca.* 456.7 eV; and (iv) at *ca.* 459.1 eV the $Ti^{4+}$ signal is observed.[14,45,46] The relative intensity of these peaks is strongly dependent on the employed chemical process for the synthesis of the investigated samples. In particular, it can be observed that all the etching processes give rise to a situation where titanium atoms are more oxidized, in agreement with the redox reactions 1–3.

The C spectra of all the samples are dominated by the signal of the MXene (282 eV), proposed as the indicator of the presence of the Ti−C network.[44] Other signals in the 284–288 eV region are related to the presence of impurities and oxidized species;[14,44,45] such impurities are observed for all the considered samples. In particular, these peaks can be attributed to: (i) $sp^3$ C atoms of adventitious carbon at *ca.* 284.8 eV; (ii) oxidized C−O carbon functionalities at *ca.* 286.0 eV; (iii) C=O carbons at *ca.* 287.2 eV; and (iv) O−C=O carbonate functional groups at *ca.* 289.4 eV.[14,44,45] It is interesting to observe that $HBF_4$ and NaF_HCl samples show the lowest content of carbon-based impurities. Moreover, in NaF_HCl the dominant contribution to carbon contaminants are in the oxidized form. This is an indication that the synthetic route adopted to obtain the MXene samples strongly affect also the residues deposited onto the surface of active particles. Nevertheless, it must be pointed out that XPS analyses give a picture of only the surface of the analyzed material, which is often non-representative of the bulk composition.

Considering the F spectral region, a unique peak is associated to the MXene (685 eV, data shown in Figure 4) and the small minor contribution can be related to $TiO_{2-x}F_{2x}$ species and/or NaF as surface residue of the etching process. Thus, for all the prepared MXene the F terminations are present and cannot be excluded. As widely accepted, it is not possible to obtain pure compositions (e.g., $Ti_3C_2F_2$ and $Ti_3C_2O_2$) using etching procedures always leading to the introduction of different terminations. From the O region, the trend derived for the T composition from the analysis of the Ti portion is confirmed. Indeed, two peaks have been attributed to the C−Ti−O and C−Ti−OH/C−Ti−F moieties at 529.8 and 532.0 eV, respectively, while the 530.8, 533.4 and 534.6 eV peaks are associated with presence of $TiO_{2-x}F_{2x}$, oxidized carbon functionalities and adsorbed $H_2O$.[44,47]

The XPS analysis thus confirms the presence of the Ti−C skeleton, the F/O mixed composition for the termination, but also the presence of intercalated species. Indeed, for the MX_$NH_4HF_2$ sample is observed the highest nitrogen content (3.4 at%, associated to impurities for the other samples) and associated to $NH_4^+$ moieties intercalated within the layers that can explain the high interplanar distance determined from XRD analysis (1.23 nm).[31] Similarly, the presence of chloride ions as termination and/or intercalated species are revealed for the MX_$NaBF_4$_HCl samples (3.7 at% vs no detection for other samples) for which the highest interplanar distance has been determined (1.37 nm), while the presence of Na is detected for the MX_NaF_HCl samples (26.2 at%) with associated d 1.05 nm. The observed trend in the interplanar distance follow the trend in the ionic radii of the considered ionic species ($Na^+$ 1.02 Å, $NH_4^+$ 1.48 Å, $Cl^-$ 1.81 Å). All the considered samples are thus comparable in terms of purity, elemental composition, and morphology to the MX_$HF_{5\%}$ reference samples. At the same

**Table 3.** Elemental analysis (CHNS) of the MXenes.

| Sample | C [%w] | H [%w] | N [%w] | S [%w] |
|---|---|---|---|---|
| MX_$NH_4HF_2$ | 10.99 | 0.58 | 0.61 | 0.12 |
| MX_NaF_HCl | 10.47 | 0.61 | 0.00 | 0.21 |
| MX_$HBF_4$ | 10.65 | 0.55 | 0.00 | 0.07 |
| MX_$NaBF_4$_HCl | 9.47 | 0.61 | 0.00 | 0.21 |
| MX theoretical | 11.85 | 0.00 | 0.00 | 0.00 |

**ChemElectroChem**

Research Article
doi.org/10.1002/celc.202200891

**Chemistry Europe**
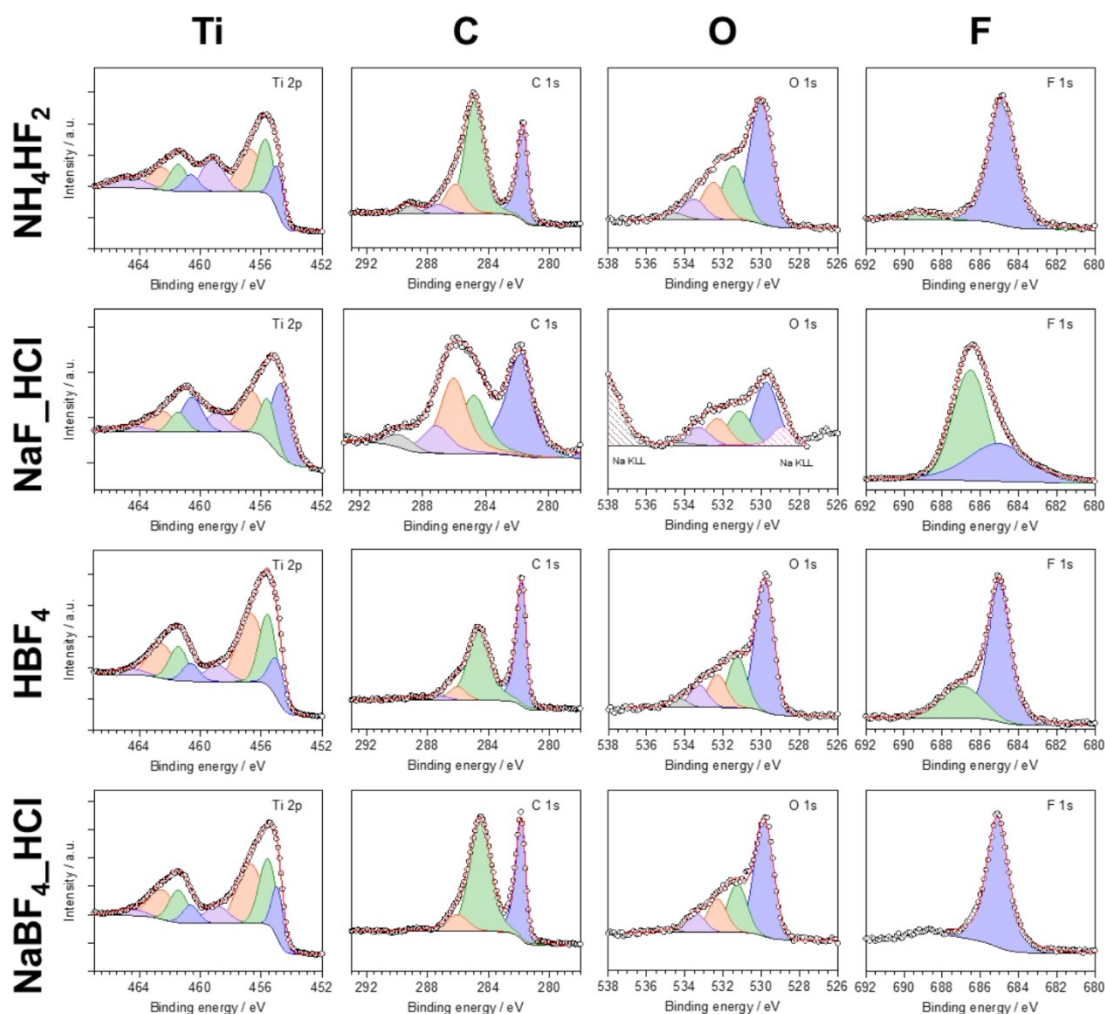European Chemical
Societies Publishing

**Figure 4.** Selected portions (Ti, C, O, F) of the XPS spectra acquired for the four samples considered in this study.

time all the samples present higher interplanar distance with respect to the MX_HF$_{5\%}$ composition thus being very promising for application as anode for sodium ion batteries. For these reasons, all the materials have been tested; results are reported in Figure 5.

The charge and discharge profiles, in Figure 5a, show that all MXenes show a pseudocapacitive behavior. All materials have a sloping potential for most of the explored range and, with the exception of MX_NaBF$_4$_HCl, a small plateau around 2.2 V indicating a biphasic electrochemical process,[48] already observed in the literature in MXenes produced with low concentrations of HF. All the materials show significant charge loss during the first cycle. The profiles are different for each composition such as the degree of the irreversibility, thus different mechanism and reactions must be inferred. This is consistent with the different impurities and intercalated species detected from the XPS analysis discussed above. A contribution of the irreversibility is coming from the formation of the solid electrolyte interphase, SEI, on the surface of the lamellae, electrochemical process that occurs on the electrode below 1 V vs Na$^+$, and by a partial irreversible intercalation of sodium, as

widely discussed in the literature.[44] Despite the possibility of remedying this inefficiency by means of chemical or electrochemical pretreatments, the first cycle coulombic efficiency is a quantitative parameter that allows the active material to be judged qualitatively. In this regard, the MX_NH$_4$HF$_2$, MX_NaF_HCl, MX_HBF$_4$ and MX_NaBF$_4$_HCl have first cycle efficiency of 36.9, 57.7, 69.7, and 55.4%, respectively. MX_HBF$_4$ therefore shows a value that is not only better than the other treatments, but also higher than the standard etching procedure in 5% HF (67%).[14]

To further characterize the electrochemical performance, the C-rate tests have been performed, and results are reported in Figure 5b. All the materials tend to stabilize after 4–5 cycles, this can be seen from the efficiency which converges over 99%. Specific capacity varies between the materials: considering the capacities delivered at 15 mAg$^{-1}$ between cycles 60–70 we obtain an average capacity of 115 mAhg$^{-1}$ for MX_NH$_4$HF$_2$, 100 mAhg$^{-1}$ for MX_NaF_HCl, 96 mAhg$^{-1}$ for MX_HBF$_4$, and 83 mAhg$^{-1}$ for MX_NaBF$_4$_HCl. The values reported for the first two materials are similar with those reported in the literature for MXenes produced under the same conditions[14] and for our
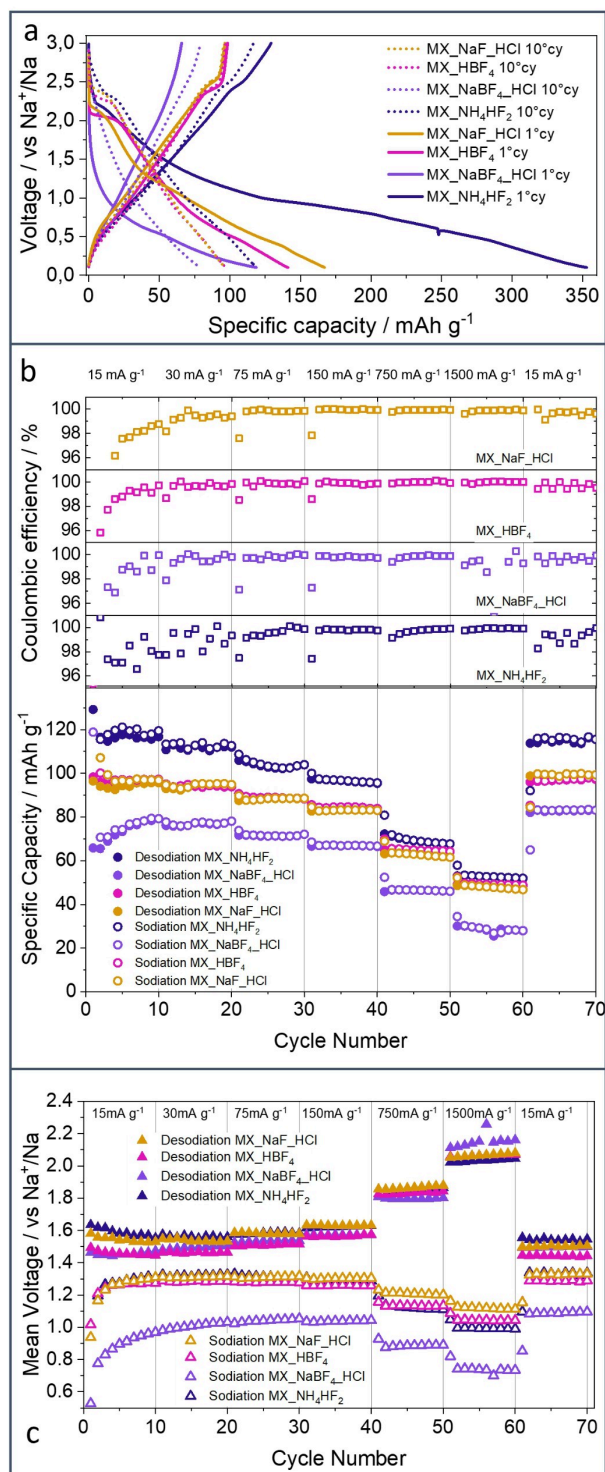
**Figure 5.** (a) Charge-discharge profile of MXenes in half cell vs sodium. (b) The cycling performance: specific capacity and coulombic efficiency, in the C-rate test. The current used are: 15, 30, 75, 150, 750, 1500, and 15 mA g$^{-1}$. (c) Mean voltage in the cycling.

lower capacity than the other materials in all current ranges explored. This decrease could be related to the peculiar crystal structure of this sample, which is characterized by a multimodal distribution of interlayer distances, as shown in Figure 2. In fact, as already demonstrated, the reduced crystal order is responsible for lower electrochemical performance.[14] Although the evaluation of capacity retention during a long cycle is not the purpose of this work, we can see that all materials show no decrease in capacity at the end of the test, the first and 70th cycle anodic values being practically the same. However, this result is in line with the literature, where it has been shown that $Ti_3C_2T_x$ is one of the negative electrodes for the Na Ion Batteries, NIBs, with the longest lifetime in full cells.[36]

Finally, the average potential in sodiation and desodiation has been evaluated (Figure 5c). It has been calculated as the ratio between the energy of the cell and the obtained capacity. The potential hysteresis increases with the current during C-rate test due to the increase in overvoltages. The mean voltage, calculated between 60–70 cycles in desodiation, that is when the MXene works as an anode in the battery. The obtained values are between 1.44 V and 1.54 V for the considered samples, being extremally promising for their application. Indeed, for a considered anodic material it is very important to show the lowest possible average potential because in a full cell it allows to exploit different cathodes. Among the considered materials, the best is $MX\_HBF_4$, which has both the lowest mean voltage and the lowest potential hysteresis. On the contrary, $MX\_NaBF_4\_HCl$ has the greatest potential hysteresis between charge and discharge due to a large overvoltage in the intercalation process of sodium in its structure.

## Conclusion

We reported here the comparison among different etching techniques considered as alternative to the direct use of HF etching. Three of the proposed methods have already been reported but here optimized, allowing for a direct comparison. The last one is here reported for the first time. Different techniques have been exploited to characterize the main aspects associated to the structure, composition, and morphology. The results reveals that all the considered solutions can successfully produce MXenes powders under the considered experimental mild conditions avoiding the direct use of HF. While the morphology is similar and differ only for the more or less pronounced lamellar structure, the produced MXenes are characterized by different interplanar distance, strongly dependent on the termination and moieties intercalated during the synthesis (e.g., $Na^+$, $NH_4^+$); the composition varies similarly due to the etching media that influence both the termination composition and the presence of possible intercalated moieties. All these aspects have a role in determining the electrochemical performances and tailoring the peculiar properties in terms of delivered capacity, irreversibility, average potential. The best results are shown by the MXene obtained with the newly introduced etching solution, i.e., the $HBF_4$ based etching medium. Indeed, while the delivered capacity is 96 mAh g$^{-1}$ and

reference composition.[36] The capacity of $MX\_HBF_4$ is in line with these two MXenes, so it is possible to define that the etching in this acid is equivalent to other conventional and standard etching in the literature. The $MX\_NaBF_4\_HCl$ has a

**ChemElectroChem**

Research Article
doi.org/10.1002/celc.202200891

**Chemistry Europe**
European Chemical
Societies Publishing

thus slightly lower than the value obtained for the MX_HF$_{5\%}$ standard, it shows low average potential and the best capacity retention reported by our group. The overall performances are thus comparable to the reference MX_HF$_{5\%}$, produced with the conventional methods using HF. Although the obtained final products are similar, the two etching agents are characterized by huge differences in terms of harmfulness and minima safety requirements both at laboratory and industrial scale. Indeed, while the HBF$_4$ is labelled as dangerous and has hazard statements associated with skin burns, HF is categorized as dangerous, fatal if swallowed, in contact with skin or inhaled. The newly proposed method is thus emerging among the considered in-situ HF forming processes as the most suitable for the sustainable, scalable, and easy production of MXene under mild conditions (24 h, 40 °C, water solution), opening the way for the massive production of such material.
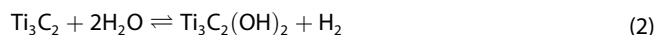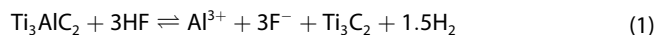
## Experimental Section

### MAX phase synthesis

The Ti$_3$AlC$_2$ MAX phase has been obtained using the spark plasma sintering (SPS) method; this procedure has been already widely considered for the synthesis of this class of materials.[9,49,50] The SPS promotes the reaction of the starting mixture and the densification of the final product exploiting low temperature and shorter time comparted to traditional hot pressing/solid state synthesis.

A mixture of Ti, Al, TiC has been prepared in molar ratio 1:1:1.9; the off stoichiometry has been optimized to minimize the TiC as secondary phases in the final product.[51] The starting powders have been mixed in a Turbula shaker for 24 h, and then heated at 1300 °C (heating rate of 80 °C/min) with mechanical load for 5 minutes and compressive load of 43 MPa, using 300 mbar of Ar pressure in the SPS chamber. The obtained material has been finely grounded and the fraction with particle size $< 50\ \mu m$ has been considered for the etching procedures.

### MXene synthesis

The etching reaction is based on the presence of HF, formed in situ. As reference, the traditional HF etching is here reported. The etching reaction can be resumed with three steps occurring simultaneously that can be described using Equation 1–3:[32]

$$Ti_3AlC_2 + 3HF \rightleftharpoons Al^{3+} + 3F^- + Ti_3C_2 + 1.5H_2 \tag{1}$$

$$Ti_3C_2 + 2H_2O \rightleftharpoons Ti_3C_2(OH)_2 + H_2 \tag{2}$$

$$Ti_3C_2 + 2HF \rightleftharpoons Ti_3C_2F_2 + H_2 \tag{3}$$

The speed of the etching increases with the concentration of HF in solution. The complete etching of the MAX phase requires, in fact, from 5 to 24 hours decreasing the HF concentration from 30% to 5%, respectively.[31] When the in-situ HF generation approach is used, the reaction times are longer ranging from 24 to 48 hours. The duration of the treatment here reported has been optimized to maximize the yields of MXene.

### Preparation of the solutions

The etching protocols are very similar to each other. The synthesis scheme is showed in Figure 1b. For all the preparation and etching procedures Teflon labware has been used. Four aqueous solutions are prepared with the following chemical species:

– NH$_4$HF$_2$ at 10 wt%,

– NaF + HCl in composition 8.5 wt% + 18 wt%,

– HBF$_4$ at 20 wt%

– NaBF$_4$ + HCl in composition 10 wt% + 18 wt%.

The four aqueous solutions produce HF in situ with the following reactions:
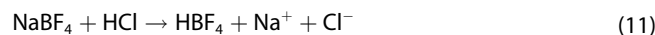
**Etching solution 1**[32]

$$NH_4HF_2 \rightleftharpoons NH_4^+ + HF + F^- \tag{4}$$

$$HF + H_2O \rightleftharpoons F^- + H_3O^+ \tag{5}$$

**Etching solution 2**[31]

$$NaF + HCl \rightarrow HF + Na^+ + Cl^- \tag{6}$$

$$HF + H_2O \rightleftharpoons F^- + H_3O^+ \tag{7}$$

**Etching solution 3**[52]

$$HBF_4 \rightleftharpoons HF + BF_3 \tag{8}$$

$$BF_3 + 3H_2O \rightleftharpoons 3HF + H_3BO_3 \tag{9}$$

$$HF + H_2O \rightleftharpoons F^- + H_3O^+ \tag{10}$$

**Etching solution 4**[33]

$$NaBF_4 + HCl \rightarrow HBF_4 + Na^+ + Cl^- \tag{11}$$

$$HBF_4 \rightleftharpoons HF + BF_3 \tag{12}$$

$$BF_3 + 3H_2O \rightleftharpoons 3HF + H_3BO_3 \tag{13}$$

$$HF + H_2O \rightleftharpoons F^- + H_3O^+ \tag{14}$$

While the use of etching solutions 1, 2, and 4 have been already reported for the etching of MAX phase, the solution 3 has never been considered before. Moreover, here we standardize the conditions for the MXene preparation thus the products obtained for the four procedures are directly comparable. The maximum nominal amount of HF that can be obtained for the four solutions has been calculated for a comparison with the traditional direct HF etching; results are listed together with the samples in Table 1.

### Etching procedure

The etching solutions have been prepared according to the stoichiometry reported above; 500 mg of Ti$_3$AlC$_2$ (particle size under 50 μm) has been slowly added to avoid temperature peaks. Indeed, even if direct hydrofluoric acid is not used, its formation in solution can be fast. The reaction with the MAX phase is exothermic and quick involving significant heating and /or violent production of gas bubbles. The controlled addition of powders to the solution is

**ChemElectroChem**

Research Article
doi.org/10.1002/celc.202200891

**Chemistry Europe**
European Chemical
Societies Publishing

needed to avoid these effects that can alter the composition and morphology of the final products. The solutions are kept at 40–60 °C in an oil bath depending on the etching solution. After 24 h, they are washed and centrifuged several times at 9000 rpm for 10 min until the pH of the supernatant become about 6. The powders are collected in a watch glass and vacuum dried at 80 °C overnight. The samples obtained are nabbed after the etching solution, the complete list is presented in Table 1. Although it is not possible to calculate an accurate reaction yield because it isn't possible to define an exact stoichiometry for the samples obtained, a yield was calculated as:

$$(MXene\_mass)/(MAX\ phase\_mass) \times 100 \qquad (15)$$

This formula is commonly used in the literature for these materials,[53] results for each composition are reported in Table 1 together with labeling of the samples, experimental conditions, and the nominal HF concentration.

### Powder characterizations

#### XRD

The crystal structure was studied by a powder X-ray diffraction system. The instrument was Rigaku Miniflex 600 diffractometer equipped with a monochromator and a Cu Kα radiation ($\lambda = 0.15406$ nm). A step scan of 0.02 deg. and a scan rate of 1 deg.$\cdot$min$^{-1}$ were used. For the measurement of the parameter c the Bragg relation was used.

#### SEM

The image at high resolution of the powders was obtained with a Zeiss Gemini SEM electron microscope.

#### CHNS

The elemental analysis for the quantification of carbon, hydrogen and nitrogen (CHNS) was done with Elementar - vario MACRO cube.

#### XPS

The X-ray photoelectron (XPS) investigations were performed by means of a Specs EnviroESCA instrument using an AlKα excitation source (h$\upsilon = 1486.6$ eV), working at an operating pressure of ca. 10–6 mbar. Survey spectra were acquired in the binding energy (BE) range between 0 and 1460 eV, collecting data at 100 eV pass energy, 1.0 eV$\cdot$step-1, and 0.1 sec$\cdot$step-1. High resolution scans were acquired at 30 eV pass energy, 0.1 eV$\cdot$step-1, and 0.2 s$\cdot$step-1. XPS curves (BE uncertainty $= \pm 0.2$ eV) were fitted using the Keystone software of Specs and applying a Shirley-type background function. The sensitivity factors of integrated peak areas used for atomic percentages (at.%) quantification were supplied by Specs.

### Preparation and characterization of electrodes

The electrode preparation has been based on the following procedure. The active material, super P carbon and poly(acrylic acid) (PAA) were mixed in composition 8:1:1 (weight ratio). The mixture was mixed 1 h at 1000 rpm with an IKA Ultra-Turrax T-50 Homogenizer using N-methyl- 2-pyrrolidone as solvent. The dispersion was distributed on aluminum foil (MTI, thickness 15 μm) with a thickness of 10 mils (254 μm) using a doctor blade. The

coating was dried for 12 h under vacuum at 120 °C, and then calendared. Disc electrodes were cut with a diameter of 16 mm, and the mass load of active material was around 1.5–2 mg cm$^{-2}$.

The electrochemical measurements were carried out in 2-electrode cells, i.e., half coin cell CR2032 (Hohsen Corp.) assembled in argon atmosphere (H$_2$O < 0.1 ppm, O$_2$ < 0.1 ppm) in glove box. Metallic sodium was used as a counter electrode and reference while the electrolyte, supported on a glass fiber separator (Whatman®), was 1 M NaPF$_6$ in ethylene carbonate (EC)/diethyl carbonate (DEC) in ratio 1:1 vol%. The C-rate tests were performed using the following 7 current steps 15, 30, 75, 150, 750, 1500, and 15 mA g$^{-1}$. The first 10 cycles and the last 10 cycles were useful to compare the stability of the material after the high currents. The instrument was a multichannel Bio-Logic VMP3.

## Conflict of Interest

The authors declare no conflict of interest.

## Data Availability Statement

The data that support the findings of this study are available from the corresponding author upon reasonable request.

**Keywords:** anode material · electrode · HF free etching · Mxene · sodium ion batteries

[1] A. Di Bartolomeo, *Nanomaterials* **2020**, *10*, 1.
[2] N. Kurra, M. Alhabeb, K. Maleski, C. H. Wang, H. N. Alshareef, Y. Gogotsi, *ACS Energy Lett.* **2018**, *3*, 2094.
[3] L. Lavagna, G. Meligrana, C. Gerbaldi, A. Tagliaferro, M. Bartoli, *Energies* **2020**, *13*, 4867.
[4] S. Ahmad, I. Ashraf, M. A. Mansoor, S. Rizwan, M. Iqbal, *Nanomaterials* **2021**, *11*, 1.
[5] C. Ferrara, A. Gentile, S. Marchionna, R. Ruffo, *Curr. Opin. Electrochem.* **2021**, *29*, 100764.
[6] R. B. Rakhi, B. Ahmed, M. N. Hedhili, D. H. Anjum, H. N. Alshareef, *Chem. Mater.* **2015**, *27*, 5314.

[7] C. Shi, M. Beidaghi, M. Naguib, O. Mashtalir, Y. Gogotsi, S. J. L. Billinge, *Phys. Rev. Lett.* **2014**, *112*, 125501.

[8] O. Salim, K. A. Mahmoud, K. K. Pant, R. K. Joshi, *Mater. Today Chem.* **2019**, *14*, 100191.

[9] Y. Gogotsi, B. Anasori, *ACS Nano* **2019**, *13*, 8491.

[10] R. Lotfi, M. Naguib, D. E. Yilmaz, J. Nanda, A. C. T. van Duin, *J. Mater. Chem. A* **2018**, *6*, 12733.

[11] B. Libro Anasori, M. R. Lukatskaya, Y. Gogotsi, B. Anasori, M. R. Lukatskaya, Y. Gogotsi, *Nat. Rev. Mater.* **2017**, *2*, 16098.

[12] M. Benchakar, L. Loupias, C. Garnero, T. Bilyk, C. Morais, C. Canaff, N. Guignard, S. Morisset, H. Hurand, P. Chartier, J. Pacaud, V. Mauchamp, M. W. Barsoum, A. Habrioux, S. Célérier, *Appl. Surf. Sci.* **2020**, *530*, 147209.

[13] M. Li, J. Lu, K. Luo, Y. Li, K. Chang, K. Chen, J. Zhou, J. Rosen, L. Hultman, P. Eklund, P. O. Å. Persson, S. Du, Z. Chai, Z. Huang, Q. Huang, *J. Am. Chem. Soc.* **2019**, *141*, 4730.

[14] A. Gentile, C. Ferrara, S. Tosoni, M. Balordi, S. Marchionna, F. Cernuschi, M. Kim, H. Lee, R. Ruffo, *Small Methods* **2020**, *4*, 2000314.

[15] Y. Wu, P. Nie, J. Wang, H. Dou, X. Zhang, *ACS Appl. Mater. Interfaces* **2017**, *9*, 39610.

[16] B. Tang, Y. Yang, Y. Shi, H. Nie, H. Xia, X. Shen, *Polym. Compos.* **2021**, *42*, 2010.

[17] Y. Fan, D. Chen, X. Liu, G. Fan, B. Liu, *Int. J. Hydrogen Energy* **2019**, *44*, 29297.

[18] A. D. Handoko, S. N. Steinmann, Z. W. Seh, *Nanoscale Horiz.* **2019**, *4*, 809.

[19] L. Wei, C. Xiong, H. R. Jiang, X. Z. Fan, T. S. Zhao, *Energy Storage Mater.* **2020**, *25*, 885.

[20] Y. Lee, J. H. Ahn, H.-Y. Park, J. Jung, Y. Jeon, D.-G. Lee, M.-H. Kim, E. Lee, C. Kim, Y. Kwon, H.-W. Lee, J. H. Jang, J. H. Lee, H.-K. Song, *Nano Energy* **2021**, *79*, 105363.

[21] I. Ihsanullah, *Nano-Micro Lett.* **2020**, *12*, 1.

[22] P. Srimuk, F. Kaasik, B. Krüner, A. Tolosa, S. Fleischmann, N. Jäckel, M. C. Tekeli, M. Aslan, M. E. Suss, V. Presser, *J. Mater. Chem. A* **2016**, *4*, 18265.

[23] J. Pang, R. G. Mendes, A. Bachmatiuk, L. Zhao, H. Q. Ta, T. Gemming, H. Liu, Z. Liu, M. H. Rummeli, *Chem. Soc. Rev.* **2019**, *48*, 72.

[24] S. Arnold, A. Gentile, Y. Li, Q. Wang, S. Marchionna, R. Ruffo, V. Presser, *J. Mater. Chem. A* **2022**, *10*, 10569.

[25] S. Kajiyama, L. Szabova, K. Sodeyama, H. Iinuma, R. Morita, K. Gotoh, Y. Tateyama, M. Okubo, A. Yamada, *ACS Nano* **2016**, *10*, 3334.

[26] C. E. Shuck, A. Sarycheva, M. Anayee, A. Levitt, Y. Zhu, S. Uzun, V. Balitskiy, V. Zahorodna, O. Gogotsi, Y. Gogotsi, *Adv. Eng. Mater.* **2020**, *22*, 1.

[27] T. Li, L. Yao, Q. Liu, J. Gu, R. Luo, J. Li, X. Yan, W. Wang, P. Liu, B. Chen, W. Zhang, W. Abbas, R. Naz, D. Zhang, *Angew. Chem. Int. Ed.* **2018**, *57*, 6115.

[28] P. Urbankowski, B. Anasori, T. Makaryan, D. Er, S. Kota, P. L. Walsh, M. Zhao, V. B. Shenoy, M. W. Barsoum, Y. Gogotsi, *Nanoscale* **2016**, *8*, 11385.

[29] Y. Li, H. Shao, Z. Lin, J. Lu, L. Liu, B. Duployer, P. O. Å. Persson, P. Eklund, L. Hultman, M. Li, K. Chen, X. H. Zha, S. Du, P. Rozier, Z. Chai, E. Raymundo-Piñero, P. L. Taberna, P. Simon, Q. Huang, *Nat. Mater.* **2020**, *19*, 894.

[30] S. Husmann, Ö. Budak, H. Shim, K. Liang, M. Aslan, A. Kruth, A. Quade, M. Naguib, V. Presser, *Chem. Commun.* **2020**, *56*, 11082.

[31] M. Alhabeb, K. Maleski, B. Anasori, P. Lelyukh, L. Clark, S. Sin, Y. Gogotsi, *Chem. Mater.* **2017**, *29*, 7633.

[32] J. Halim, M. R. Lukatskaya, K. M. Cook, J. Lu, C. R. Smith, L. Å. Näslund, S. J. May, L. Hultman, Y. Gogotsi, P. Eklund, M. W. Barsoum, *Chem. Mater.* **2014**, *26*, 2374.

[33] C. Peng, P. Wei, X. Chen, Y. Zhang, F. Zhu, Y. Cao, H. Wang, H. Yu, F. Peng, *Ceram. Int.* **2018**, *44*, 18886.

[34] H. Wang, M. Godara, Z. Chen, H. Xie, *Sens. Actuators A Phys.* **2019**, *290*, 130.

[35] J. Y. Lin, A. Raharjo, L. H. Hsu, Y. J. Shih, Y. H. Huang, *Water Res.* **2019**, *155*, 362.

[36] C. Ferrara, A. Gentile, S. Marchionna, I. Quinzeni, M. Fracchia, P. Ghigna, S. Pollastri, C. Ritter, G. M. Vanacore, R. Ruffo, *Nano Lett.* **2021**, *21*, 8290.

[37] J. Peng, X. Chen, W. J. Ong, X. Zhao, N. Li, *Chem* **2019**, *5*, 18.

[38] T. Hu, M. Hu, B. Gao, W. Li, X. Wang, *J. Phys. Chem. C* **2018**, *122*, 18501.

[39] S. Liu, L. Wang, X. Wang, L. Liu, A. Zhou, X. Cao, *Mater. Today Commun.* **2020**, *22*, 100799.

[40] S. Célérier, S. Hurand, C. Garnero, S. Morisset, M. Benchakar, A. Habrioux, P. Chartier, V. Mauchamp, N. Findling, B. Lanson, E. Ferrage, *Chem. Mater.* **2019**, *31*, 454.

[41] A. Feng, Y. Yu, F. Jiang, Y. Wang, L. Mi, Y. Yu, L. Song, *Ceram. Int.* **2017**, *43*, 6322.

[42] M. Khazaei, A. Ranjbar, M. Arai, T. Sasaki, S. Yunoki, *J. Mater. Chem. C* **2017**, *5*, 2488.

[43] M. Khazaei, A. Mishra, N. S. Venkataramanan, A. K. Singh, S. Yunoki, *Curr. Opin. Solid State Mater. Sci.* **2019**, *23*, 164.

[44] V. Natu, M. Benchakar, C. Canaff, A. Habrioux, S. Célérier, M. W. Barsoum, *Matter* **2021**, *4*, 1224.

[45] J. Halim, K. M. Cook, M. Naguib, P. Eklund, Y. Gogotsi, J. Rosen, M. W. Barsoum, *Appl. Surf. Sci.* **2016**, *362*, 406.

[46] S. Myhra, J. A. A. Crossley, M. W. Barsoum, *J. Phys. Chem. Solids* **2001**, *62*, 811.

[47] A. A. Iurchenkova, E. V. Lobiak, A. A. Kobets, A. N. Kolodin, A. Stott, S. R. P. Silva, E. O. Fedorovskaya, *Electrochim. Acta* **2021**, *370*, 137832.

[48] X. Wang, S. Kajiyama, H. Iinuma, E. Hosono, S. Oro, I. Moriguchi, M. Okubo, A. Yamada, *Nat. Commun.* **2015**, *6*, 1.

[49] Y. Mizuno, K. Sato, M. Mrinalini, T. S. Suzuki, Y. Sakka, *J. Ceram. Soc. Jpn.* **2013**, *121*, 366.

[50] B. Anasori, Y. Gogotsi, in *2D metal carbides and nitrides (MXenes) for energy storage*, Springer, **2019**.

[51] Y. Zou, Z. M. Sun, H. Hashimoto, S. Tada, *J. Alloys Compd.* **2008**, *456*, 456.

[52] Z. Lai, F. Peng, Y. Wang, H. Wang, H. Yu, P. Liu, H. Zhao, *J. Mater. Chem.* **2012**, *22*, 23906.

[53] M. Naguib, O. Mashtalir, J. Carle, V. Presser, J. Lu, L. Hultman, Y. Gogotsi, M. W. Barsoum, *ACS Nano* **2012**, *6*, 1322.